Energy Materials and Devices

Research Article

Detailed computational modeling of crack patterns of silicon-based anode sheet in lithium-ion batteries upon mechanical stress

Yuzuki Kawashima, Kazuma Ogata, Yuto Shibayama, Aoi Takagi, Akio Yonezu ✉, and Jun Xu ✉

Graphical Abstract

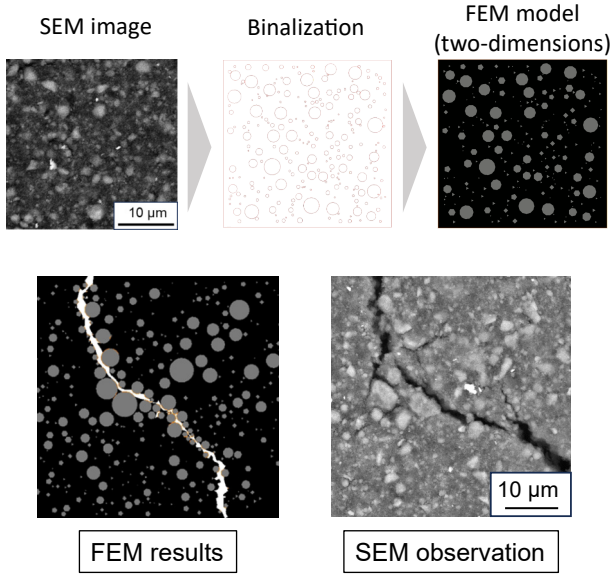

In this work, finite element modeling incorporating the Oyane failure criterion was used to simulate and validate microcrack initiation and propagation in silicon-based anodes, linking computational results to experimental scanning electron microscopy observations. This approach provides a pathway to optimize microstructural designs for enhanced performance and durability in lithium-ion batteries.

✉Address correspondence to
Akio Yonezu, yonezu@mech.chuo-u.ac.jp;
Jun Xu, junxu@udel.edu

Received: November 15, 2024
Revised: December 10, 2024
Accepted: December 30, 2024

Citation: Kawashima Y., Ogata K., Shibayama Y., et al. Detailed computational modeling of crack patterns of silicon-based anode sheet in lithium-ion batteries upon mechanical stress. *Energy Mater. Devices*, 2025, 3(3), 9370054. https://doi.org/10.26599/EMD.2025.9370054

Energy Materials and Devices

Open Access

Research Article

https://doi.org/10.26599/EMD.2025.9370054

Detailed computational modeling of crack patterns of silicon-based anode sheet in lithium-ion batteries upon mechanical stress

Yuzuki Kawashima[1], Kazuma Ogata[1], Yuto Shibayama[1], Aoi Takagi[1], Akio Yonezu[1] ✉, and Jun Xu[2,3] ✉

[1] *Department of Precision Mechanics, Faculty of Science and Engineering, Chuo University, Tokyo 1128551, Japan*
[2] *Department of Mechanical Engineering, University of Delaware, Newark, DE 19716, USA*
[3] *Energy Mechanics and Sustainability Laboratory (EMSLab), University of Delaware, Newark, DE 19716, USA*

Received: November 15, 2024 / **Revised:** December 10, 2024 / **Accepted:** December 30, 2024

ABSTRACT

Silicon (Si)-based anodes, where Si serves as the active material, have garnered significant attention due to their potential to achieve high electric capacity in lithium-ion batteries (LIBs). A key challenge with Si-based anodes is their susceptibility to create in-plane cracks caused by stresses from the manufacturing process and cyclic charging, which ultimately shortens battery life and reduces the overall electrochemical capacity. To address this issue, a refined microstructural design of the active material layer is in pressing need to enhance both the performance and longevity of LIBs. We successfully applied the Oyane failure criterion, which models ductile failure under stress triaxiality, to simulate crack initiation and propagation in the binder matrix containing Si particles in the finite element modeling. Given the non-linear plastic deformation of the binder, this criterion was formulated based on cumulative strain increments. The computational results of microcrack formation within the active material layer under uniaxial tension were then validated by the experimental observations. Furthermore, we developed several models with varied particle arrangements, comparing each simulated crack path to actual microstructural images obtained via scanning electron microscopy. The findings confirm the accuracy of the model, underlying its promising application in optimizing the microstructure of Si-based anodes for enhanced LIB performance and durability.

KEYWORDS

lithium-ion battery (LIB), microcracking, crack criteria, finite element method (FEM), Si-based anode, binder

1 Introduction

Lithium-ion batteries (LIBs) have become the cornerstone of energy storage for modern applications, spanning portable electronics, electric vehicles, and large-scale energy storage systems[1–3]. The global demand for higher energy density and improved battery performance has driven extensive research into alternative electrode materials. In this pursuit, silicon (Si)-based anodes are highly promising due to Si's high theoretical specific capacity (3579 mAh/g), which significantly exceeds that of traditional graphite anodes (372 mAh/g)[4,5]. However, the incorporation of Si as an anode material has introduced new mechanical and electrochemical challenges, primarily associated with its volumetric expansion (up to 300%) and the resultant mechanical stresses. These factors often lead to cracking and subsequent degradation of the anode, reducing the capacity retention and cycling life of the battery[6,7].

This volumetric expansion generates substantial internal stresses that exceed the fracture strength of both Si particles and the surrounding binder matrix, leading to crack formation and propagation within

✉Address correspondence to Akio Yonezu, yonezu@mech.chuo-u.ac.jp; Jun Xu, junxu@udel.edu

the anode[6,8,9]. Repeated lithiation and delithiation cycles exacerbate these stresses, causing progressive mechanical degradation and the formation of microcracks, which impede the effective transport of lithium ions and electrons, thereby diminishing the anode's structural integrity and electrochemical performance[10–12]. To address these issues, a detailed understanding of the crack initiation and propagation mechanisms in Si-based anodes is essential for developing robust, high-performance LIBs.

Experimental studies using techniques such as scanning electron microscopy (SEM) and transmission electron microscopy have provided valuable insights into the microstructural evolution of Si anodes during cycling, revealing patterns of crack formation, particle fracture, and binder debonding[13,14]. However, these experiments are often limited by spatial and temporal resolution constraints, making it challenging to capture real-time crack propagation at the microscale[6]. Consequently, computational modeling has emerged as a powerful tool for investigating the mechanical behavior of Si-based anodes, enabling detailed analysis of stress distributions, crack patterns, and failure modes under various cycling conditions[15,16]. The finite element method (FEM) has been particularly effective for simulating the interaction between Si particles and the binder matrix, providing insights into stress concentration, crack initiation, and propagation[17]. Notably, simulations incorporating cohesive zone models and damage mechanics have demonstrated how stress concentration around Si particles leads to localized cracking within the binder matrix, ultimately contributing to overall anode degradation[17–20].

While FEM provides a foundational framework for understanding the mechanical behavior of Si-based anodes, accurately modeling crack patterns requires incorporating realistic damage criteria that can capture the complexities of ductile fracture within the binder. The Oyane criterion, a commonly used damage model, accounts for ductile failure due to stress triaxiality, making it well-suited for materials that undergo significant plastic deformation[21]. This criterion has been applied in various studies to simulate ductile fracture in composite materials, and its application to Si-based anodes offers potential for simulating crack initiation and propagation with high accuracy. By integrating the Oyane failure criterion into FEM, we can account for stress triaxiality-driven void nucleation and growth, providing a more accurate representation of microcrack formation and evolution in the Si–binder matrix under tensile and cyclic loading conditions.

Despite advancements in FEM and damage mechanics for Si anodes, challenges remain in accurately predicting crack patterns due to the inherent variability in Si particle size, shape, and distribution, as well as the stochastic nature of crack propagation. Studies have shown that small variations in particle arrangement can lead to significantly different stress distributions and crack paths, suggesting that a probabilistic approach may be necessary for a comprehensive understanding of crack formation[22]. Furthermore, experimental validation of computational models remains essential, as discrepancies between simulated and observed crack patterns highlight the need for improved model accuracy and parameterization[23]. High-resolution imaging techniques, such as SEM and focused ion beam microscopy, are invaluable for validating crack patterns and stress distributions predicted by FEM simulations, reinforcing the relevance of integrated experimental–computational studies[24,25].

In this study, we aim to develop a comprehensive computational model of crack patterns in Si-based anodes by employing the Oyane failure criterion within a FEM framework. By simulating the stress distribution and crack initiation around Si particles under uniaxial tension, we seek to replicate observed crack paths and validate our model against experimental data from SEM imaging. Additionally, we examine the influence of particle arrangement on stress concentration and crack propagation, providing a detailed understanding of the structural factors that affect the durability of Si-based anodes. Our approach not only advances the modeling of mechanical degradation in LIBs but also offers practical insights for optimizing the microstructure of Si-based anodes to enhance performance and extend battery life.

2 Experiment

2.1 Specimen

In this study, a commercially available Si-based anode sheet was used as the primary material. The specimen consists of a dual-layer structure with an active material layer deposited on a 10 μm thick copper (Cu) foil, which serves as the current collector (Fig. 1). The active material layer has a thickness of 34 μm and is composed of pure Si particles as the active material with average size of 0.5 μm, combined with a binder made from poly(acrylic acid) and styrene-butadiene rubber (PAA-SBR). This composite structure results in a complex, hierarchical microstructure within the anode sheet, which presents unique challenges for understanding and modeling its mechanical properties. To isolate and better understand the mechanical behavior of the binder matrix itself, we also prepared a "binder sheet" by coating the Cu foil with the binder material alone, excluding the Si particles. This binder-only layer

serves as a control to directly assess the mechanical contribution of the binder without interference from the active material.

Mechanical properties of the anode sheet, Cu current collector, and binder layer were characterized through a series of experimental tests, including uniaxial tensile testing and nanoindentation. These tests provided essential data on the elastic and plastic properties, hardness, and stiffness of each component. These mechanical characterizations are critical inputs for developing a FEM, which is discussed in subsequent sections, to simulate the mechanical responses of the Si-based anode under operational stresses.

Through this approach, the study aims to provide a detailed understanding of how each layer and material component contributes to the overall mechanical behavior of the anode, thereby informing improvements in the design and performance of Si-based anodes for high-energy-density batteries.

2.2 Uniaxial tension

To investigate the mechanical properties and fracture behavior of the Si-based anode sheet, with a particular focus on the active material layer (34 μm in thickness), uniaxial tensile tests were performed on the entire anode sheet. All tensile tests were conducted using a universal testing machine (Autograph AG-1, Shimadzu Corporation) with displacement control set to 0.1 mm/min (quasi-static loading). Dumbbell-shaped specimens were prepared according to Japanese industrial standards 7137-2-A standards. Strain was measured using a non-contact digital image correlation device to ensure high accuracy in capturing deformation characteristics. The anode sheet exhibited a higher peak load, which can be attributed to the reinforcing effect of the Si particles in the active material layer (Fig. 2a). However, the fracture displacement of the anode sheet was lower than that of the Cu foil, indicating that the Si-based anode layer is relatively brittle compared to the Cu substrate though it exhibited certain degrees of plasticity. The results also suggest that when cracking initiates within the active material layer, stress concentration occurs at the interface between the active layer and the Cu foil, accelerating the failure of the Cu substrate itself. This interface-driven crack propagation ultimately leads to the complete structural failure of the anode sheet. These findings offer valuable parameters for the FEM efforts described in subsequent sections, contributing to a more robust understanding of the mechanical stability of Si-based anode structures under operational conditions.

We conducted a detailed investigation of the free surface around the fracture plane of the active material layer to gain insights into its macroscopic fracture morphology and the role of Si particles in fracture behavior. For a comprehensive analysis, we also examined the fracture characteristics of a binder-only sheet without Si particles, allowing us to isolate and compare the effects of the active material. SEM images of the fracture surfaces illustrate clear distinctions in fracture behavior between the binder layers with and without embedded Si particles (Fig. 2b). The fracture surface of the active material layer containing Si particles reveals a markedly brittle fracture mode (Fig. 2b). The surface appears relatively flat and smooth, with few indications of plastic deformation around the Si particles. This morphology indicates that the Si particles disrupt the binder's ability to deform plastically, acting instead as stress concentrators that localize stress and create weak points within the matrix. When subjected to tensile loading, these stress concentrations lead to abrupt crack initiation at the Si/binder interfaces, resulting in rapid crack propagation through the active layer. The presence of Si particles, therefore, transforms the fracture mode from ductile to brittle, as the particles hinder the binder's ductile flow and facilitate a lower-energy, more catastrophic failure pathway.

In contrast, the fracture surface of the binder-only sheet, which exhibits features characteristic of ductile failure, including localized necking and fibrillation of the binder matrix (Fig. 2b). These features suggest

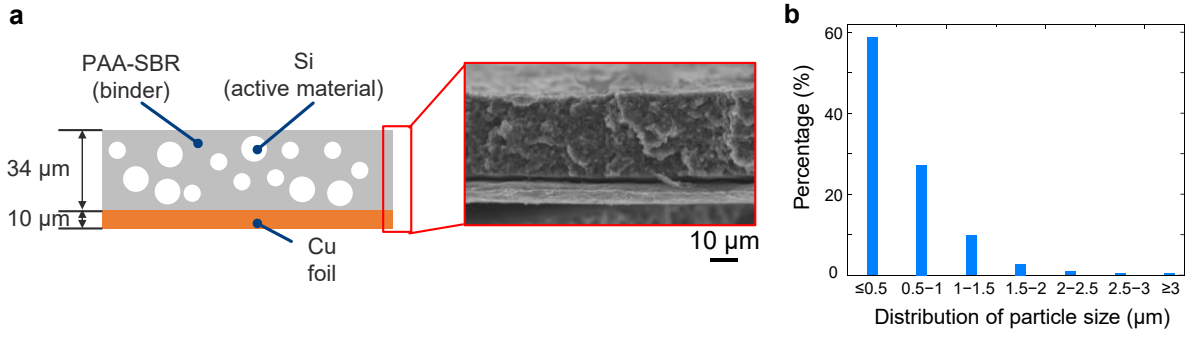

Figure 1 (a) Schematic cross-sectional view of the Si-based anode sheet. The hierarchical microstructure of the active material layer is designed to balance mechanical stability and electrochemical activity, with the Cu foil providing structural support and efficient electron transport. (b) The schematic highlights the thickness, material composition, and arrangement of the different layers.

significant plastic deformation prior to fracture, as the binder undergoes stretching and elongation at the fracture front. This ductile behavior indicates that the binder alone can absorb strain energy and redistribute stress effectively, enabling plastic deformation and resisting crack initiation under tensile loading.

To understand the mechanics of crack initiation and propagation around the Si particles in greater detail, we conducted additional SEM observations at higher magnifications, focusing on the interfaces between the Si particles and the binder matrix. We observed micro-cracks forming at the particle/matrix interface, which suggests that the mismatch in mechanical properties (*e.g.*, elastic modulus and fracture toughness) between Si and the binder promotes stress localization (Fig. 2c). The rigid Si particles cannot accommodate the strains imposed by the surrounding binder under tensile stress, causing the interface to act as a nucleation site for cracks. These cracks propagate more easily along the Si/binder interfaces, where the cohesive strength is comparatively lower, accelerating the overall fracture process and leading to a ductile–brittle response on the macroscopic scale.

SEM images of the active material layer surface reveal microcrack propagation patterns, with cracks traveling along Si particle boundaries in a characteristic zigzag path, highlighting how Si particles act as stress concentrators that promote microcrack initiation and growth (Fig. 2c). In contrast, the binder-only sheet shows no evidence of microcracks, displaying instead a ductile fracture morphology similar to that shown previously (Fig. 2b). These SEM images were taken near the fracture surface after tensile testing, capturing the microcracks in the active material layer that emerge just before the specimen's final failure. As microcracks accumulate and coalesce, they lead to complete fracture, as observed in the overall morphology of the fractured surface (Figs. 2b and 2c). This progression underscores the importance of microstructural design in LIB anodes, where the distribution and interface quality of Si particles within the binder matrix play a pivotal role in governing crack initiation and propagation.

2.3 Nanoindentation

Furthermore, nanoindentation tests were performed on both the binder matrix and Si-rich regions to quantify their respective elastoplastic properties, including hardness, Young's modulus, and yield strength. These properties are crucial for our FEM analysis as they provide the necessary parameters to model the differential strain accommodation between the Si particles and the binder matrix. To develop the FEM model, it was essential to determine the elastoplastic properties of the binder. Nanoindentation tests were conducted using a dynamic ultra micro hardness tester (DUH201, Shimadzu Corporation) with a Berkovich indenter under force control at a rate of 0.146 mN/s. The resulting force–displacement curves for the binder layer were recorded. Each test was repeated five times, with the average data shown for consistency.

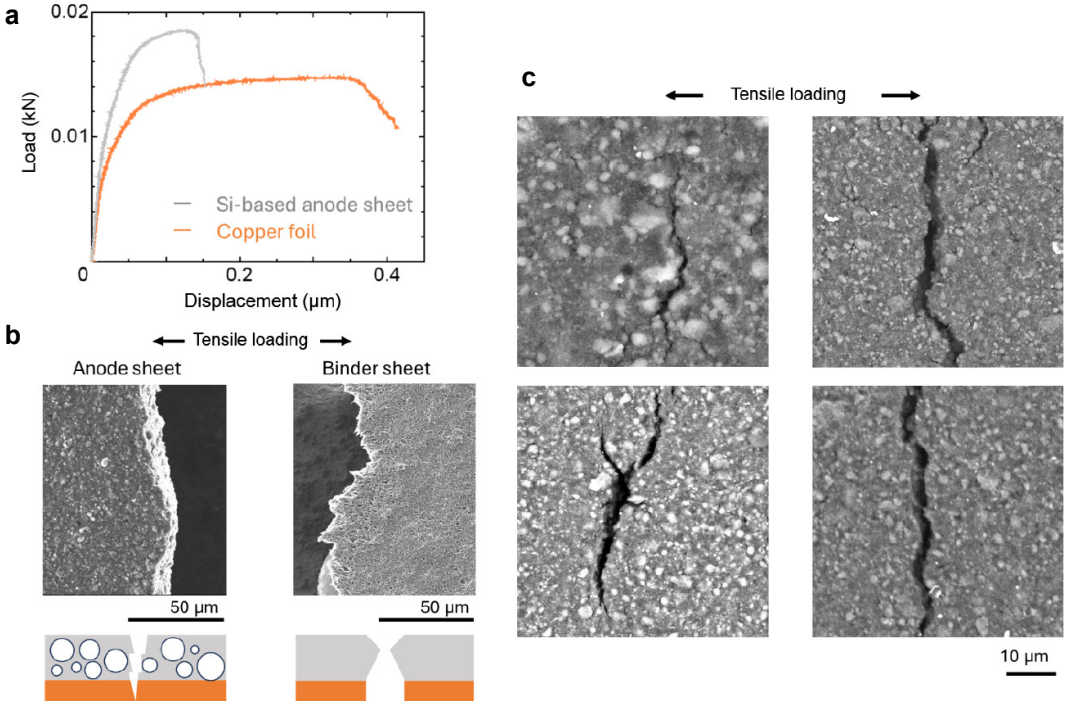

Figure 2 (a) Tensile load–displacement curves for the full Si-based anode sheet and the Cu foil current collector. (b) The fracture surfaces of Si-based anode sheet and binder sheet. (c) Four examples of SEM images of crack propagations in active material layer.

The Oliver–Pharr method[21] was employed to evaluate the contact area of the indenter and to determine the Young's modulus E of the binder layer, assuming a Poisson's ratio of 0.35 (Fig. 3). Using the contact area from this analysis, the hardness of the binder was calculated, providing an estimate of the yield stress, as 29 and 30 MPa for the active material layer and binder layer with Young's modulus of 8.7 and 4.8 GPa, respectively. The data reveal that Young's modulus of the active material layer, which contains hard Si particles, is significantly higher than that of the binder layer alone. This increase is attributed to the stiffening effect of the Si particles within the binder matrix. In contrast, the yield strength of the active material layer is comparable to that of the binder-only layer, likely due to the fact that yielding initiates within the binder matrix, which has a much lower strength compared to the Si particles. These mechanical property distinctions provide crucial input parameters for accurately simulating the stress and deformation behavior of the anode's active material layer in the FEM model.

3 FEM simulation

To better predict and understand these crack formation and propagation behaviors, which are influenced by the spatial alignment and bonding of Si particles, this study established an FEM model of the active material layer. This FEM approach enables simulation of stress distribution and crack propagation, providing valuable insights into the impact of particle alignment and binder properties on fracture mechanics where such predictive capability is essential for optimizing the microstructural design of high-energy-density LIB anodes, ultimately enhancing their durability and performance.

3.1 Failure criteria

Since fracture behavior and failure criteria can vary significantly depending on the material's properties, we first analyzed the fracture behavior and microcracking mechanisms within the polymer binder. The experimental observations (Fig. 2b) reveal that the fracture surface of the active material layer exhibits brittle characteristics when Si particles are present, while the binder-only layer shows a more ductile fracture surface. This contrast in fracture behavior underscores the need for an accurate failure criterion that reflects the ductile nature of the binder material.

To capture this behavior in the FEM model, we applied the Oyane failure criterion, which is effective in representing ductile fracture mechanisms. By integrating this criterion, the model is able to simulate crack initiation and propagation within the binder, closely mirroring the experimentally observed fracture patterns.

The Oyane failure rule describes a phenomenon in which the formation of micro void is governed by the stress triaxiality and is expressed by the following equation[7–9]

$$\int_0^{\varepsilon_f} \left(\frac{\sigma_m}{\bar{\sigma}} + a \right) d\varepsilon \leq b \tag{1}$$

this equation involves two material parameters (a and b) and stress triaxiality (mean stress σ_m, equivalent stress $\bar{\sigma}$, fracture strain ε_f and equivalent strain ε). The left-hand side of Eq. (1) calculates the incremental strain corresponding to the stress triaxiality, thus obtaining the damage value. This variation in damage value is referred to as the fracture index. When the left-hand side of the fracture index exceeds a pre-set threshold b, element deletion occurs, representing damage evolution within the model. In this simulation, crack initiation and propagation are

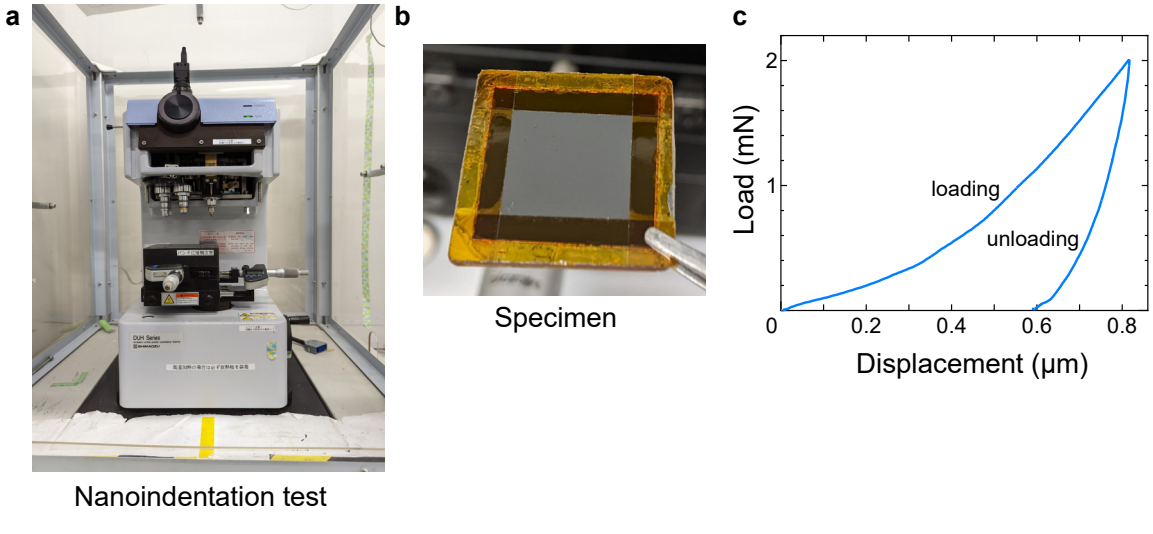

Figure 3 Schematic representation of the nanoindentation equipment (a) and testing specimens (b), highlighting the indenter geometry and specimen preparation process. (c) The load–displacement curve obtained during nanoindentation highlights the loading, holding, and unloading phases, which provide insights into mechanical properties such as hardness and elastic modulus.

modeled through element deletion. The FEM mesh size is much smaller than the Si particles, allowing for accurate reproduction of microcrack propagation behavior by calibrating two parameters, a and b, in Eq. (1). These parameters are determined from experimental results of tensile loading tests on two specimens with different stress triaxialities. Quantitative values for a and b are optimized through FEM simulations to replicate the tensile loading behavior of both specimens and are validated by comparison with experimental data.

To introduce distinct stress triaxialities, we used both dumbbell-shaped and notched specimens (Fig. 4). FEM simulations of tensile deformation were performed for both specimen types to generate load–displacement curves. The FEM models were constructed to match the exact geometries of the experimental specimens, allowing for realistic three-dimensional (3D) elastoplastic simulations.

It is important to note that these simulations were conducted without including the failure criterion, solely to highlight the differences in stress triaxiality (Fig. 4). The endpoint of each curve corresponds to the fracture displacement observed experimentally. Results indicate a strong dependence of stress triaxiality on specimen geometry. The notched specimen exhibits higher stress triaxiality due to the biaxial tension induced by its notched shape, resulting in a shorter elongation at fracture in the load–displacement curve. This difference in stress and strain states for the two specimen types is expected to yield unique values for parameters a and b in Eq. (1) (where $a = 0$ and $b = 0.011$), capturing the influence of geometry-dependent stress triaxiality on fracture behavior.

3.2 Pre-treatment for the modeling

For simplicity, a two-dimensional microstructural model was employed instead of a full 3D model. This choice was based on the thickness of the active material layer (35 μm in thickness) and the dominance of surface crack morphology since the crack pattern is highly influenced by the microstructure, specifically the arrangement, size, and distribution of particles.

To accurately reproduce the microstructure of the active material layer, the FEM model was constructed based on the particle arrangement and size derived from SEM images of the anode sheet (Fig. 5). First, an SEM image of the anode sheet surface was captured, providing detailed information on particle distribution. This image was then binarized to extract precise particle locations and sizes, which were used to define the FEM model's geometry. For computational simplicity, each particle in the FEM model was approximated as a perfect circle (or sphere in 3D). This modeling approach enabled a realistic representation of the microstructural features, allowing us to investigate the effects of particle arrangement on

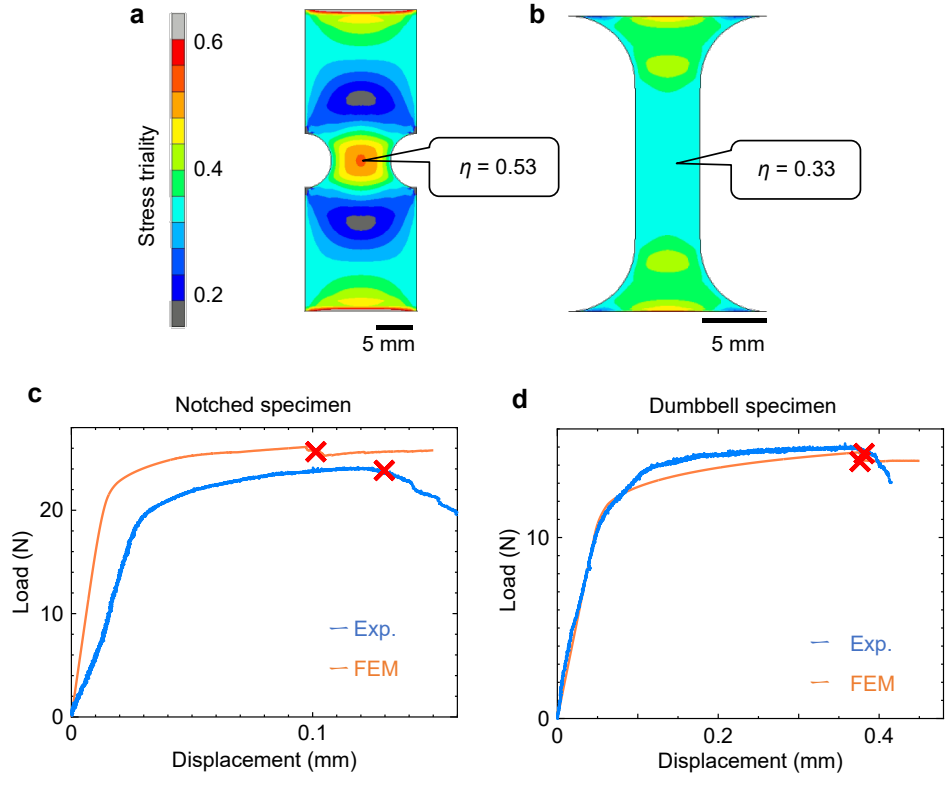

Figure 4 Schematic of the specimen with notched shape (a) and dumbbell shape (b), and their load–displacement curves from both experiments and FEM analysis ((c) and (d)).

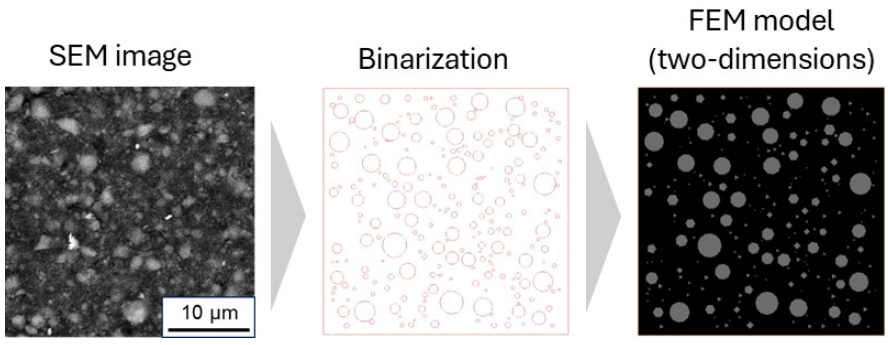

Figure 5 Step-by-step creation process of FEM modeling to replicate the microstructure in the active material layer of battery electrodes.

microcrack initiation and propagation within the active material layer.

The Oyane failure criterion was applied within the FEM model to simulate microcrack propagation, utilizing the mechanical properties of the binder material, as mentioned above. To capture microstructural effects accurately, the representative volume element (RVE) size was set between 30 μm × 30 μm and 50 μm × 50 μm, and periodic boundary conditions were implemented on all sides to ensure that the model reflects the continuity of the material's microstructure. A uniaxial tensile load was applied to simulate the stress conditions that the material undergoes during operation, focusing on the localized crack propagation behavior under tensile stress. The Cu foil substrate was excluded from this analysis to isolate the crack pattern and path induced specifically by tensile loading within the binder and active material phase. The detailed modeling not only addresses macroscopic stress values or the critical stress levels for crack initiation and propagation due to the inherently local nature of the microstructural model (Fig. 5), which represents only a fraction of the bulk material.

3.3 Model results

The simulation results suggest that the interference of stress concentration by the particles promotes crack formation with a complicated path. Furthermore, the crack propagates in a zigzag manner. The ease of stress concentration, i.e., crack initiation and propagation, is considered to depend on factors such as inter-particle distance, relative position of particles, and particle size. Stress concentration is more likely to occur when the distance between particles is close and the particle size is large for both tensile and perpendicular to tensile directions. Such a systematic study can be conducted using our developed FEM model.

Three distinct crack propagation patterns were observed experimentally, each corresponding to a unique microstructural configuration (Fig. 6). To match these, two RVE sizes were designated: 50 μm × 50 μm (denoted as RVE50 for Models 1 and 2) and 30 μm × 30 μm (denoted as RVE30 for Model 3). The results reveal a significant dependence of crack morphology on particle arrangement, including particle size distribution, interparticle spacing, and binder phase thickness. These factors impact the stress distribution within the binder and active material, which, in turn, affects the crack initiation sites and propagation paths.

For each RVE, the microstructural arrangement leads to distinct stress concentration zones where microcracks preferentially initiate. In regions with high particle density and minimal binder thickness, stress concentration tends to localize, facilitating crack coalescence and accelerating propagation. Conversely, in regions with larger interparticle distances, crack bridging within the binder is more prominent, leading to a more tortuous crack path. These variations in crack path morphology align closely with SEM observations (Fig. 6), indicating the model's ability to predict realistic crack propagation patterns. Additionally, by adjusting the material parameters for the binder, we observed sensitivity in crack growth rates, particularly in response to changes in binder stiffness and ductility. A stiffer binder material led to faster crack initiation due to reduced energy dissipation, while a more ductile binder delayed crack growth, as it absorbed greater deformation energy. These observations underscore the importance of optimizing binder properties to control crack propagation in practical engineering applications.

3.4 Model validations and discussions

We verified our FEM model by assessing the degree of agreement between the particle configuration in the model and that observed in SEM images. To quantify this agreement, we evaluated the particle arrangement using a segmented analysis (Fig. 7a). First, each SEM image was divided into five horizontal segments. For each segment, the position of each particle was recorded based on the center coordinates, allowing us to count the number of particles

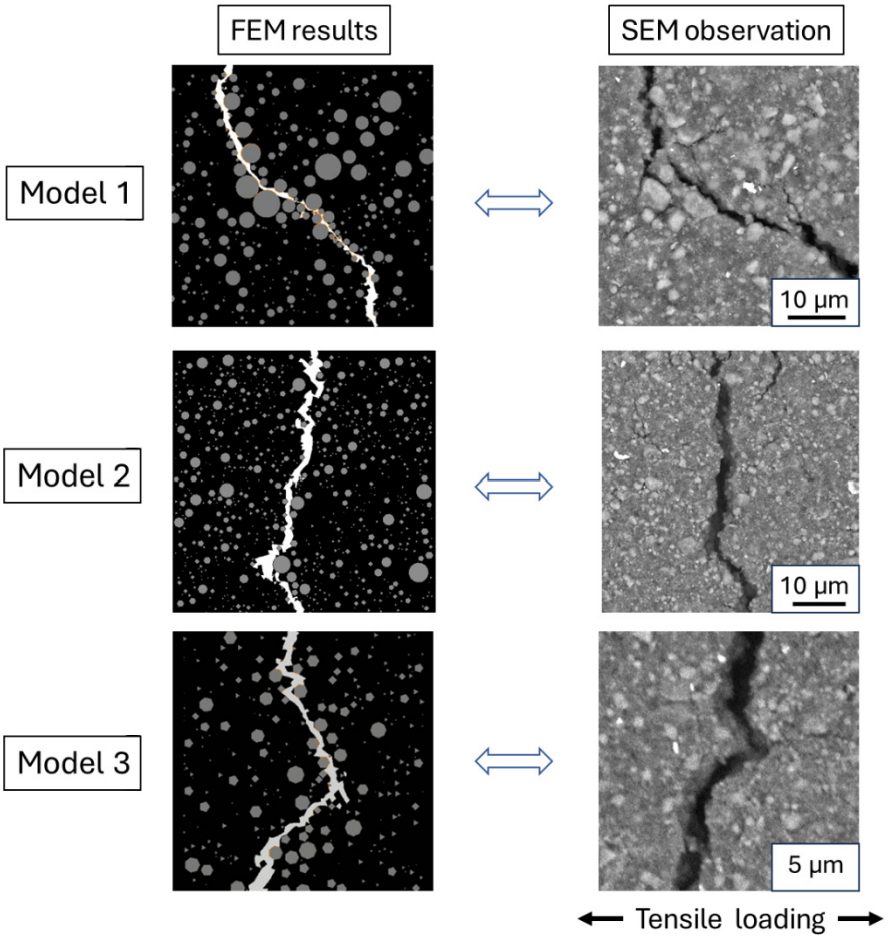

Figure 6 Simulation of the crack propagation in active materials for three patterns of the cracks observed from SEM images.

within each segment. In Model 1 (RVE50) (Fig. 6), for example, each segment had a width of 10 μm. The particle ratio in each segment was then calculated as a percentage of the total particle count within the entire RVE size. This segmented particle distribution was compared with that in the SEM images, providing a quantitative measure of particle arrangement similarity between the model and experimental observations.

These small error values indicate a high level of consistency between the particle configurations in the SEM images and the FEM models for all three models (Fig. 7b). This agreement confirms that our FEM models accurately replicate the particle arrangements observed in the actual Si-based anode sheets, supporting the model's validity for further mechanical and microstructural analyses. The strong agreement between FEM model predictions and experimental crack patterns demonstrates that this FEM model can effectively capture microstructural influences on crack initiation and propagation under tensile loading conditions.

Our FEM model successfully predicts a complex crack pattern in the active material layer. The simulation results indicate that the interaction of stress concentrations around Si particles promotes crack formation along an intricate, non-linear path. The cracks propagate in a characteristic zigzag manner, which highlights the impact of local stress fields influenced by the microstructural arrangement of particles. The initiation and propagation of these cracks appear to be highly dependent on factors such as inter-particle distance, particle positioning, and particle size. Specifically, stress concentration is more likely to develop when particles are closely spaced and larger in size, increasing the likelihood of crack formation both along the tensile direction and perpendicular to it. This suggests that particle configurations with reduced spacing and larger particles create stress hotspots, enhancing the probability of crack initiation and irregular propagation paths.

4 Conclusion

The active material layer of the anode sheet plays a crucial role in the overall performance and durability of LIBs. It is well-documented that both the manufacturing process and repeated charge–discharge cycles induce multiple cracks within the binder matrix of this layer. This study presents a FEM modeling framework to simulate microcrack initiation and propagation in the active material layer of

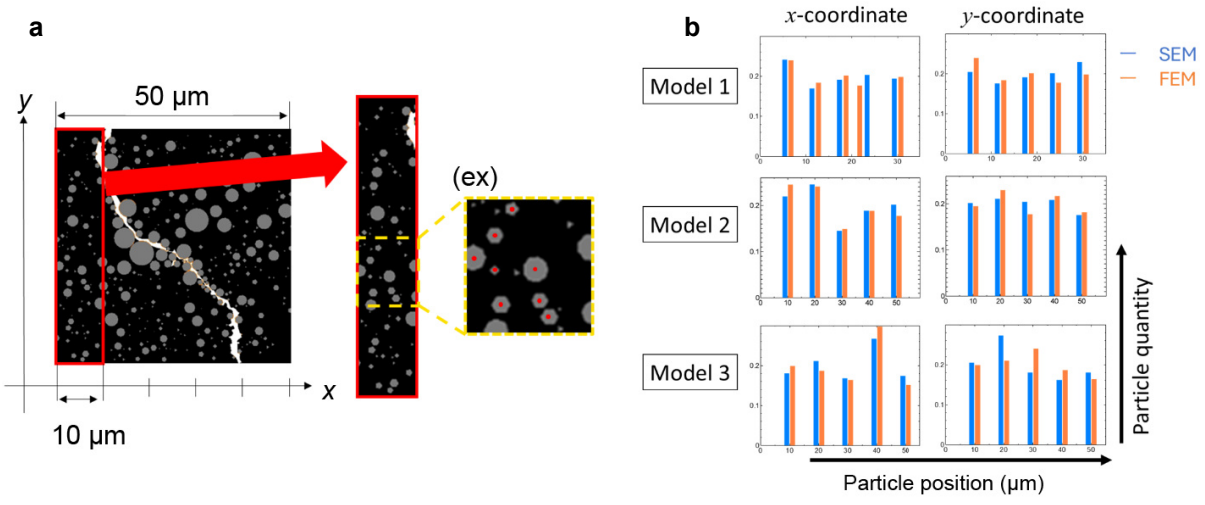

Figure 7 (a) Process for evaluating particle configurations to achieve experimental similarity. (b) Comparative analysis of particle configuration similarity in FEM model and SEM image.

LIBs anodes, with a specific focus on Si-based active materials. Our model captures the intricate crack patterns arising from stress concentration around Si particles embedded in a polymeric binder. By constructing a microstructural model based on experimentally observed particle distributions and applying the Oyane failure criterion, we successfully replicated the complex, zigzagging crack paths that develop under uniaxial tensile loading.

The results demonstrate that crack initiation and propagation in the active material layer are highly sensitive to particle size, spatial arrangement, and inter-particle distances. These insights underline the critical role of microstructural design in managing crack behavior within the binder matrix, directly influencing the mechanical stability and long-term performance of LIBs. Our model not only provides a predictive tool for understanding failure mechanisms but also offers actionable guidelines for optimizing particle configuration and binder properties to enhance anode resilience against mechanical degradation.

This work paves the way for a systematic, design-driven approach to anode architecture that mitigates crack formation in high-energy-density batteries. Our findings offer a foundation for advancing LIB design, with the potential to drive improvements in both cycle life and safety in next-generation energy storage systems.

Acknowledgements

None.

Author contribution statement

Yuzuki Kawashima: Methodology, modeling, data analysis, and writing – original draft; Kazuma Ogata: Experiment and data analysis; Yuto Shibayama: Experiment and data analysis; Aoi Takagi: Data analysis; Akio Yonezu: Methodology, supervision, and writing – review & editing; Jun Xu: Conceptualization, methodology, supervision, and writing – review & editing. All the authors have approved the final manuscript.

Data availability

All the data has been included in the paper.

Declaration of competing interest

Jun Xu is one of the editorial board member of this journal and the editor of the current special issue, but he was not involved in the peer review or decision of this article. The other contributing author reports no conflicts of interest in this work.

Funding

Akio Yonezu acknowledges the support of JSPS KAKENHI (Grant No. 21H01217) from the Japan Society for the Promotion of Science. Jun Xu acknowledges the support of the Startup funds from the University of Delaware.

Use of AI statement

None.

References

[1] Xie, J., Lu, Y. C. (2020). A retrospective on lithium-ion batteries. *Nat. Commun.* 11, 2499.

[2] Liu, B. H., Jia, Y. K., Yuan, C. H., Wang, L. B., Gao, X., Yin, S., Xu, J. (2020). Safety issues and mechanisms of lithium-ion battery cell upon mechanical abusive loading: a review. *Energy Storage Mater.* 24, 85–112.

[3] Gao, X., Chak, C., Hao, Q., Zeng, D., Xu, J. (2023). Ther-

mal safety of lithium-ion batteries: mechanism, modeling, and characterizations. *Annu. Rev. Heat Transfer* 26, 69–129.

[4] Liu, T., Dong, T. T., Wang, M. Y., Du, X. F., Sun, Y. L., Xu, G. J., Zhang, H. R., Dong, S. M., Cui, G. L. (2024). Recycled micro-sized silicon anode for high-voltage lithium-ion batteries. *Nat. Sustain.* 7, 1057–1066.

[5] Kim, N., Kim, Y., Sung, J., Cho, J. (2023). Issues impeding the commercialization of laboratory innovations for energy-dense Si-containing lithium-ion batteries. *Nat. Energy* 8, 921–933.

[6] Gao, X., Jia, Y. K., Zhang, W., Yuan, C. H., Xu, J. (2022). Mechanics-driven anode material failure in battery safety and capacity deterioration issues: a review. *Appl. Mech. Rev.* 74, 060801.

[7] Gao, X., Xu, J. (2024). Carbon binder domain inhomogeneity in silicon-monoxide/graphite composite anode by 2D multiphysics modeling. *Adv. Sci.* 11, 2400729.

[8] Gross, S. J., Hsieh, M. T., Mumm, D. R., Valdevit, L., Mohraz, A. (2022). Alleviating expansion-induced mechanical degradation in lithium-ion battery silicon anodes via morphological design. *Extreme Mech. Lett.* 54, 101746.

[9] Jerliu, B., Hüger, E., Dörrer, L., Seidlhofer, B. K., Steitz, R., Oberst, V., Geckle, U., Bruns, M., Schmidt, H. (2014). Volume expansion during lithiation of amorphous silicon thin film electrodes studied by in-*operando* neutron reflectometry. *J. Phys. Chem. C* 118, 9395–9399.

[10] Feyzi, E., M R, A. K., Li, X., Deng, S. X., Nanda, J., Zaghib, K. (2024). A comprehensive review of silicon anodes for high-energy lithium-ion batteries: challenges, latest developments, and perspectives. *Next Energy* 5, 100176.

[11] Meng, T., Li, B., Liu, C., Wang, Q. S., Su, H. J., Hu, L., Hao, J. N., Du, E. P., Gu, F. L., Huang, B. B., et al. (2021). Surface engineering enables highly reversible lithium-ion storage and durable structure for advanced silicon anode. *Cell Rep. Phys. Sci.* 2, 100486 .

[12] Li, A. M., Wang, Z. Y., Pollard, T. P., Zhang, W. R., Tan, S., Li, T. Y., Jayawardana, C., Liou, S. C., Rao, J. C., Lucht, B. L., et al. (2024). High voltage electrolytes for lithium-ion batteries with micro-sized silicon anodes. *Nat. Commun.* 15, 1206.

[13] Huo, H. Y., Jiang, M., Bai, Y., Ahmed, S., Volz, K., Hartmann, H., Henss, A., Singh, C. V., Raabe, D., Janek, J. (2024). Chemo-mechanical failure mechanisms of the silicon anode in solid-state batteries. *Nat. Mater.* 23, 543–551.

[14] Zhang, L., Al-Mamun, M., Wang, L., Dou, Y. H., Qu, L. B., Dou, S. X., Liu, H. K., Zhao, H. J. (2022). The typical structural evolution of silicon anode. *Cell Rep. Phys. Sci.* 3, 100811.

[15] Bonkile, M. P., Jiang, Y., Kirkaldy, N., Sulzer, V., Timms, R., Wang, H. Z., Offer, G., Wu, B. (2024). Is silicon worth it? Modelling degradation in composite silicon–graphite lithium-ion battery electrodes. *J. Power Sources* 606, 234256.

[16] Kim, S. H., Dong, K., Zhao, H., El-Zoka, A. A., Zhou, X. Y., Woods, E. V., Giuliani, F., Manke, I., Raabe, D., Gault, B. (2022). Understanding the degradation of a model Si anode in a Li-ion battery at the atomic scale. *J. Phys. Chem. Lett.* 13, 8416–8421.

[17] Pistorio, F., Clerici, D., Mocera, F., Somà, A. (2023). Review on the numerical modeling of fracture in active materials for lithium ion batteries. *J. Power Sources* 566, 232875.

[18] Meng, X. Q., Xu, Y. L., Cao, H. B., Lin, X., Ning, P. G., Zhang, Y., Garcia, Y. G., Sun, Z. (2020). Internal failure of anode materials for lithium batteries — a critical review. *Green Energy Environ.* 5, 22–36.

[19] Ogata, K., Tan, W. X., Takano, Y., Yonezu, A., Xu, J. (2023). Mechanical characterization and modeling of microstructural deformation of Si anode sheet. *J. Power Sources* 580, 233442.

[20] Bahramifar, S., Haftbaradaran, H., Mossaiby, F. (2021). Cohesive modeling of crack formation in two-phase planar electrodes subject to diffusion induced stresses using the distributed dislocation method. *Int. J. Mech. Sci.* 194, 106183.

[21] Oyane, M., Sato, T., Okimoto, K., Shima, S. (1980). Criteria for ductile fracture and their applications. *J. Mech. Work. Technol.* 4, 65–81.

[22] Hun, D. A., Guilleminot, J., Yvonnet, J., Bornert, M. (2019). Stochastic multiscale modeling of crack propagation in random heterogeneous media. *Int. J. Numer. Methods Eng.* 119, 1325–1344.

[23] Wierzbicki, T., Bao, Y. B., Lee, Y. W., Bai, Y. L. (2005). Calibration and evaluation of seven fracture models. *Int. J. Mech. Sci.* 47, 719–743.

[24] Mammadi, Y., Joseph, A., Joulain, A., Bonneville, J., Tromas, C., Hedan, S., Valle, V. (2020). Nanometric metrology by FIB-SEM-DIC measurements of strain field and fracture separation on composite metallic material. *Mater. Des.* 192, 108665.

[25] Liu, X., Meng, S. W., Liang, Z. Z., Tang, C. A., Tao, J. P., Tang, J. Z. (2023). Microscale crack propagation in shale samples using focused ion beam scanning electron microscopy and three-dimensional numerical modeling. *Pet. Sci.* 20, 1488–1512.